ELSEVIER

Journal of Power Sources 81–82 (1999) 487–490

JOURNAL OF POWER SOURCES

www.elsevier.com/locate/jpowsour

First-principles calculation of atomic structure and electrochemical potential of $Li_{1+x}V_3O_8$

R. Benedek [a,*], M.M. Thackeray [a], L.H. Yang [b]

[a] *Electrochemical Technology Program, Chemical Technology Division, Argonne National Laboratory, Argonne, IL, USA*
[b] *Lawrence Livermore National Laboratory, Livermore, CA, USA*

Abstract

Interest in the γ-bronze, $Li_{1+x}V_3O_8$, as a possible electrode material in rechargeable Li batteries has stimulated several experimental studies on this system. Detailed interpretation of the electrochemical and physical-property measurements is complicated by uncertainties regarding the structural arrangement of Li atoms as a function of x and by a phase transition between two monoclinic structures (γ_a, γ_b) during intercalation. To elucidate the atomic structures and the phase transition, first-principles calculations are performed with the local-density-functional-theory (LDFT) planewave pseudopotential method for both γ_a and γ_b as a function of lithiation. Calculations for the compositions $1+x=1.5$ and $1+x=4$ confirm that the Li configuration determined in the existing X-ray diffraction structure refinements (at $1+x=1.2$ and $1+x=4$, respectively), coincide with the predicted low-energy configurations. Structure predictions were made at intermediate compositions, for which no experimental structure measurement is available. The order in which the tetrahedrally coordinated Li sites are filled at equilibrium as a function of x in γ_a was predicted. Calculated electrochemical potentials as a function of composition agree well with experimental data.

Keywords: Atomic structure; Lithium battery; Vanadium oxide; Modelling

1. Introduction

The structural stability of the cathode under Li insertion/extraction is critical to the performance of Li batteries, and understanding the evolution of atomic structure during lithiation is a first step toward the design of improved materials. Experimental atomic structure characterization, for example by X-ray diffraction (XRD), is limited by the availability of homogeneous specimens, and measurements have primarily been restricted to special stoichiometries at which stable, ordered compounds occur. First-principles theoretical calculations can complement experimental efforts in this regard and help to elucidate structural details of candidate battery materials. In particular, local-density functional theory [1] provides a robust framework for the parameter-free calculation of structural properties of materials. Some recent work along these lines has focused on lithiated transition-metal dioxides [2–4]. This paper presents first-principles calculations for the layered trivanadate, the so-called γ-bronze $Li_{1+x}V_3O_8$ [5], based on the planewave pseudopotential method [6,7]. The γ-bronze has a larger unit cell (25–30 atoms), and therefore requires greater computational effort than the dioxides. It has been under consideration as a possible cathode material [8–14], but its performance is degraded by a structural phase transition that occurs in the vicinity of $1+x=3$. Both the low- and high-Li phases (which we refer to as γ_a and γ_b, respectively) are monoclinic, but the former contains tetrahedrally as well as octahedrally coordinated Li. Differences between the lattice constants [5] of the two phases suggest that the transition is first order. We note that the competition between tetrahedrally and octahedrally coordinated Li in the γ_a and γ_b phases occurs in other structures as well, such as lithiated spinel $Li_{1+x}Mn_2O_4$.

2. Internal energy vs. lithiation

To elucidate the γ_a–γ_b phase transition, internal energy is calculated for both phases as a function of x. The planewave pseudopotential method [15] is well-suited to this task because it can more readily accommodate large unit cells than all-electron methods such as the full-potential linearized augmented planewave (FLAPW) method.

* Corresponding author. Tel.: +1-630-252-5063; Fax: +1-630-252-7777; E-mail: benedek@anl.gov

0378-7753/99/$ - see front matter
PII: S0378-7753(99)00208-6

The calculations are performed at the local-density-functional-theory level, and spin-polarization is neglected. Calculations for layered Li_xCoO_2 revealed [3] that total energy was negligibly affected by spin polarization, in spite of the magnetic tendencies of Co. We believe this will be the case also for the vanadium gamma bronze, but since V exhibits local moments in several compounds, we intend to perform calculations with the local-spin-density approximation in future work, as a check.

The local-density-functional-theory framework does not predict an insulating gap (except at the composition $x = 0$ [6,7], at which V is pentavalent and the octet rule is satisfied) in the electronic density of states for the trivanadate system, which is insulating at all levels of lithiation [13]. It is well known that the mean-field treatment of exchange and correlation inherent in the LDFT (or LSDFT) does not yield insulating energy gaps in many Mott–Hubbard and charge-transfer insulators. In spite of this shortcoming, structural property predictions, which are determined primarily by the electronic charge density distribution (rather than by the Fermi-shell quasiparticle properties), are often quite accurate. Some caution is warranted, of course. Metal–insulator transitions, for example, which occur in some lithiated transition metal oxides [3], are beyond the scope of LDFT. Detailed comparisons between our atomic coordinate predictions and diffraction measurements [5], however, give us confidence that our LDFT calculations for the vanadium gamma bronze are realistic.

The pseudopotential calculations employ Troullier–Martins pseudopotentials [16], a planewave cutoff energy of 70 Ry, Brillouin-zone sampling with 16 special *k*-points, and Gaussian broadening. The local exchange-correlation potential of Ceperley and Alder, as parametrized by Perdew and Zunger [17], is used.

The unit cell of $Li_{1+x}V_3O_8$ contains two formula units, with atoms located on two (010) layers stacked along the monoclinic *b*-axis; the coordinates on adjacent layers are related to each other by inversion symmetry [5]. The lattice cell vectors in most of the calculations for γ_a (γ_b) are fixed at the experimental values for $1 + x = 1.2$ (4); however, for each composition the internal coordinates are relaxed using Hellmann–Feynman forces. Both the cell vectors and the internal coordinates were relaxed for the composition $Li_4V_3O_8$ (γ_b) and the resultant cell vectors were within 2% of experimental values.

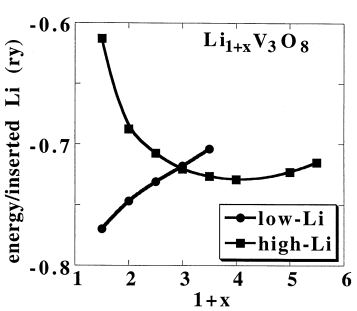

Fig. 1. Calculated total energy per inserted Li $[\Delta E = (E(1+x) - E(1))/x]$ vs. lithiation for γ_a (low-Li) and γ_b (high-Li) phases.

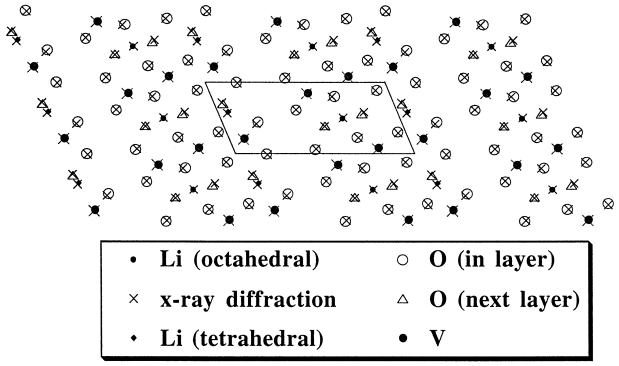

Fig. 2. Calculated and measured atomic positions for γ_a at $x = 1.5$.

A central result of this work is the energy per inserted Li as a function of composition of the two phases, which is plotted in Fig. 1. The reference composition was taken to be $x = 1$; the minimum Li content observed experimentally in this compound is 1.1–1.2. The atomic structures employed in the calculations are described in Section 3. We observe in Fig. 1 that the compositions predicted to be most stable are $x = 0+$ for γ_a and $x = 3$ for γ_b. Experimentally, these compositions (or very close to them) are the ones for which single crystal specimens are most readily synthesized and X-ray diffraction measurements are available [5]. Mean deviations of calculated relaxed atomic positions from measured values for these compositions (Fig. 2) are only about 0.15 Å. A similar level of agreement between theory and experiment is found for $Li_4V_3O_8$. The agreement between theory and experiment for the standard compounds gives us confidence in LDFT predictions for intermediate compositions.

3. Li site preference

Diffraction experiments [5] indicate that the compositions $1 + x = 1.2$ (γ_a) and $1 + x = 4$ (γ_b) are well ordered. For γ_a at the composition $1 + x = 1.2$, however, some Li disorder exists on the partially occupied Li sublattice, and such sublattice disorder is likely to exist at most compositions. Nevertheless, it appears reasonable to represent compositions with integral or half-integral by the lowest-energy ordered structure. Entropic free energy contributions are neglected in this work.

In the γ_a phase, the octahedral sites designated Li(1) are occupied in the framework structure $Li_1V_3O_8$. To test the preference for Li(1) in the framework structure, calculations at this composition were also performed with the tetrahedral site $S_1(3)$ occupied instead and the energy was found to be higher by almost 1 eV per formula unit.

Additional Li atoms ($x > 0$) in the γ_a phase are accommodated in tetrahedral sites. The most prominent tetrahe-

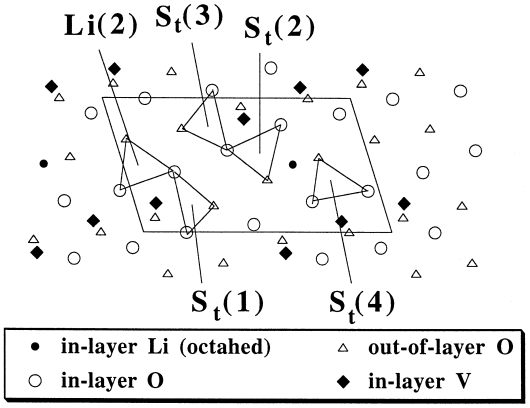

Fig. 3. Candidate tetrahedral sites in the low-Li γ_a phase. Atomic position in a layer parallel to a (010) plane; out-of-plane oxygen atoms coordinated to the in-plane Li also shown. The full unit cell comprises two such layers, whose coordinates are related by inversion symmetry.

dral sites in this structure are illustrated in Fig. 3. One of the sites labeled Li(2) is the first to be occupied, at $1+x=1.5$, but the next site to be occupied is not the other Li(2), but one of the $S_t(3)$ sites. This is followed (at $1+x=2.5$) by the other $S_t(3)$ site and then (at $1+x=3.0$) the filling of Li(2) is completed. Above $1+x=3.0$, $S_t(4)$ begins to be occupied.

In qualitative terms, the Li-filling sequence for the γ_a phase can be interpreted as follows. The structure of lithiated trivanadates is determined in general by a competition between the Li and V cations for oxygen bonds. Apart from this competition, octahedral sites with six bonds for Li would be favored over tetrahedral sites with four bonds. In the 'unintercalated' framework structure, with composition $Li_1V_3O_8$, the cation distribution is sparse enough to enable Li to occupy octahedral sites, while allowing both LiO and VO bondlengths to be close to optimal. The first intercalants into this structure, however, prefer tetrahedral Li(2) sites, which enable four strong Li–O bonds to exist without significantly distorting the V–O bonds. Tetrahedral $S_t(3)$ sites are then occupied before the filling of the Li(2) is complete, reflecting a trade-off between Li–Li repulsion and Li–O bonding (more details on this will be presented elsewhere). As more tetrahedral sites become occupied, the γ_a phase becomes less favorable than the γ_b phase, because the V–O bonds are no longer significantly less distorted than they are in γ_b, in which the Li forms six Li–O bonds.

In the γ_b phase there are five inequivalent octahedral sites for Li, as illustrated in Fig. 4. At the most stable composition, $Li_4V_3O_8$, only one of them is vacant. The most symmetric location of this vacancy is the favored site: at $S_0(2)$, with Li dimers on either side. This configuration apparently minimizes interference between Li–O and V–O bonding. Structures for γ_b with $1+x<4$ were obtained by depopulating sites in the order suggested by the vacancy energies calculated for $Li_4V_3O_8$. The composition $Li_5V_3O_8$ is obtained by filling all five sites in Fig. 4 with Li. A calculation was also done for $Li_{5.5}V_3O_8$, with an additional Li placed interstitially between layers.

4. Electrochemical potential

The differences between calculated total energies at intervals of $\Delta x=0.5$ enable (zero temperature) estimates of the Li chemical potential in the two phases of $Li_{1+x}V_3O_8$, and hence the cell electrochemical potential, which we take relative to a Li metal anode. The cell voltage is thus

$$V(x)=\mu(\text{Li, cathode})-\mu(\text{Li, anode}), \quad (1)$$

where the cathode chemical potential in a single phase region is approximated by

$$\mu(\text{Li, cathode})\approx\big(E(1+x+\Delta x/2) - E(1+x-\Delta x/2)\big)/\Delta x. \quad (2)$$

Within a two-phase region between x_a and x_b, the chemical potential

$$\mu(\text{Li, cathode})=\big(E_{\gamma_a}(x_a)-E_{\gamma_b}(x_b)\big)/(x_a-x_b) \quad (3)$$

Numerical results based on the calculated total energies for the γ_a and γ_b phases are plotted in Fig. 5 along with experimental measurements [18]. We defer discussion of the results to Section 5.

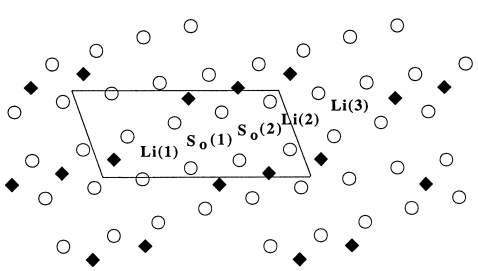

Fig. 4. Labels for Li sites in the high-Li (γ_b) phase. Atomic positions shown for a (010) layer; O (V) atoms denoted by circles (diamonds). The full unit cell comprises two such layers, whose coordinates are related by inversion symmetry.

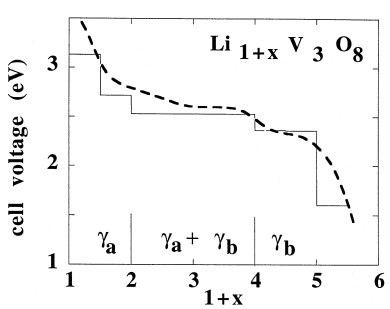

Fig. 5. Calculated (histograms) and measured electrochemical potentials for $Li_{1+x}V_3O_8$.

5. Discussion and conclusions

We have applied local-density-functional theory to calculate atomic structures and total energies for the low- and high-Li phases, γ_a and γ_b, of $Li_{1+x}V_3O_8$. The energy per inserted Li (cf. Fig. 1), a convenient measure of compound stability, was lowest for γ_a at $1+x=1.5$ and for γ_b at $1+x=4.0$. These compositions coincide closely with those for which single crystals are most readily synthesized [4].

We attribute the stability of the γ_a phase at $1+x=1.5$ to the relatively large minimum Li–Li separation, approximately 3.8 Å; the structures of γ_a phase compounds in the range $1+x=2$ to 3 have minimum Li–Li separation of about 2.5 Å. The energy plotted in Fig. 1 corresponding to $1+x=1.5$ lies below the extrapolation of a linear fit of the points at higher lithiation, an indication of the special stability of this composition.

The most stable composition of γ_b occurs at $1+x=4$. This composition corresponds to occupancy of a single *d*-electron orbital on each V^{4+} ion. It is tempting to attribute the stability of $Li_4V_3O_8$ to a Jahn–Teller effect; however, the present calculations do not include spin polarization, and hence would not incorporate the Jahn–Teller effect even if it were present in the material. The fact that the calculation nevertheless shows γ_b to be especially stable at $1+x=4$ suggests that another mechanism may be responsible for this stability. It is possible that the disparate bondlength requirements for the two types of anion–cation bonds are more readily satisfied at the composition $Li_4V_3O_8$, owing to the presence of a Li vacancy, than in $Li_5V_3O_8$, in which all cation sites are filled.

Calculated equilibrium atomic coordinates for γ_a at $1+x=1.5$ and for γ_b at $1+x=4.0$ closely agree with X-ray diffraction results. This agreement gives us confidence in the predictions made for other compositions. To understand electrochemical behavior, it is important to ascertain the phase diagram, for which no direct experimental information is available. By applying a common-tangent construction to the total energy results as a function of composition, we find a two-phase region between $1+x_a \approx 2$ and $1+x_b \approx 4$; for lithiation below $1+x \approx 2$, a single γ_a phase is predicted whereas above $1+x \approx 4$, a single γ_b phase is predicted. With these predicted (zero temperature) phase boundaries, in conjunction with Eqs. (1)–(3), we predict the electrochemical potential curve shown in Fig. 5 (histogram), which may be compared with experiment, measured under essentially open-circuit conditions (dashed curve). Close overall agreement is found between theory and experiment. One difference is that the theory predicts $1+x_a \approx 2$, whereas the plateau in the experimental curve suggests an onset of the two phase region at $1+x_a \approx 3$. Approximations invoked in the calculation, such as the neglect of variations in the lattice constant with lithiation may be partially responsible for this discrepancy. Furthermore, irreversibilities in the measured open-circuit voltage curve indicate that the insertion process does not easily produce thermodynamic equilibrium structures even at very low current. We have not addressed such irreversibilities theoretically.

Acknowledgements

We gratefully acknowledge support from the US Department of Energy Advanced Battery Research Program, Chemical Sciences Division, Office of Basic Energy Sciences. L.H.Y. was supported at Lawrence Livermore National Laboratory by the US Department of Energy under contract no. W-7405-ENG-48. Most of the computational work was performed at the National Energy Research Supercomputer Center, and at the Argonne National Laboratory IBM SP facility.

References

[1] R.O. Jones, O. Gunnarsson, Rev. Mod. Phys. 61 (1989) 689.
[2] M.K. Aydinol, A.F. Kohan, G. Ceder, Y. Cho, J. Joannopoulos, Phys. Rev. B 56 (1997) 1354.
[3] A. Van der Ven, M.K. Aydinol, G. Ceder, G. Kresse, J. Hafner, Phys. Rev. B 58 (1998) 2975.
[4] C. Wolverton, A. Zunger, Phys. Rev. B 57 (1998) 2242.
[5] L.A. de Picciotto, K.T. Adendorff, D.C. Liles, M.M. Thackeray, Solid State Ionics 62 (1993) 297.
[6] R. Benedek, M.M. Thackeray, L.H. Yang, Phys. Rev. B 56 (1997) 10707.
[7] R. Benedek, M.M. Thackeray, L.H. Yang, Mater. Res. Soc. Proceedings 496 (1998) 115.
[8] K. West, B. Zachau-Christiansen, S. Skaarup, Y. Saidi, J. Barker, I.I. Olsen, R. Pynenburg, R. Koksbang, J. Electrochem. Soc. 143 (1996) 820.
[9] J. Kawakita, H. Katagiri, T. Miura, T. Kishi, J. Power Sources 68 (1997) 680.
[10] S. Panero, M. Pasquali, G. Pistoia, J. Electrochem. Soc. 130 (1983) 1225.
[11] G. Wang, J. Roos, D. Brinkmann, M. Pasquali, G. Pistoia, J. Phys. Chem. Solids 54 (1993) 851.
[12] R. Tossici, R. Marassi, M. Berrettoni, S. Stizza, G. Pistoia, Solid State Ionics 57 (1992) 227.
[13] G. Pistoia, M. Pasquali, M. Tocci, V. Manev, R.V. Moshtev, J. Power Sources 15 (1985) 13.
[14] X. Zhang, R. Frech, Electrochim. Acta 43 (1998) 861.
[15] M.C. Payne, M.P. Teter, D.C. Allan, T.P. Arias, J.D. Joannopoulos, Rev. Mod. Phys. 64 (1992) 1045.
[16] N. Troullier, J.-L. Martins, Phys. Rev. B 43 (1991) 1993.
[17] J.P. Perdew, A. Zunger, Phys. Rev. B 25 (1981) 5048.
[18] V. Battaglia, A. Jansen, A. Kahaian, unpublished data, 1997.